ELSEVIER

Contents lists available at ScienceDirect

Physica D

journal homepage: www.elsevier.com/locate/physd



Interactions of solitary pulses of *E. coli* in a one-dimensional nutrient gradient



Glenn Young ^{a,*}, Mahmut Demir ^{b,e}, Hanna Salman ^{b,c}, G. Bard Ermentrout ^d, Ionathan E. Rubin ^d

- ^a Department of Mathematics, Pennsylvania State University, University Park, PA, USA
- b Department of Physics and Astronomy, The Dietrich School of Arts and Sciences, University of Pittsburgh, Pittsburgh, PA, USA
- ^c Department of Computational and Systems Biology, School of Medicine, University of Pittsburgh, Pittsburgh, PA, USA
- ^d Department of Mathematics, The Dietrich School of Arts and Sciences, University of Pittsburgh, Pittsburgh, PA, USA
- ^e Department of Molecular, Cellular and Developmental Biology, Yale University, New Haven, CT, USA

HIGHLIGHTS

- A two-population Keller-Segel model exhibits two qualitatively distinct behaviors.
- We derive an ODE system that represents dynamics of population spatial profiles.
- The derived system predicts how parameter changes affect outcomes.
- Experimental results reveal behaviors predicted by the model.

ARTICLE INFO

Article history: Received 23 October 2018 Received in revised form 6 February 2019 Accepted 11 February 2019 Available online 19 February 2019 Communicated by Jordi Garcia-Ojalvo

Keywords:
Keller-Segel
Chemotaxis
Pulse interaction
E. coli
Collective behavior

ABSTRACT

We study the interaction of two bacterial pulses in a one-dimensional nutrient gradient. Simulations of the Keller–Segel chemotaxis model reveal two qualitatively distinct behaviors. As the two pulses approach one another, they either combine and move as a single pulse or, surprisingly, change direction and begin moving away from each other in the direction from which they originated. To study this phenomenon, we introduce a heuristic approximation to the spatial profiles of the pulses in the Keller–Segel model and derive a system of ordinary differential equations approximating the dynamics of the pulse centers of mass and widths. This approximation simplifies analysis of the global dynamics of the bacterial system and allows us to efficiently explore qualitative behavior changes under a range of parameter variations. We end by presenting experimental data showing that populations of E. coli display behavior that qualitatively agrees with our theoretical results.

© 2019 Elsevier B.V. All rights reserved.

1. Introduction

A bacterial pulse is a common pattern of collective bacterial migration, which has been well characterized across many studies [1–5]. Pulses occur when cellular concentration is large enough for directional movement by chemotaxis (or any other form of taxis; e.g., [4]) to overcome diffusion, allowing the bacteria to concentrate into a close group [6,7]. Such collective behavior has been identified as a mechanism that provides bacteria with certain selective advantages; for example, aggregation supports the formation of biofilms, which confer protection against antibiotics and other environmental stress [8,9]. While much is known about single-pulse systems, multiple-pulse systems have received comparatively little attention. Recently, it was shown that traveling

bacterial pulses containing two species of bacteria can synchronize or bifurcate into two pulses traveling in the same direction, depending primarily on the relative speeds of the two bacterial species and on the relative abundance each species [2]. Here we consider a system in which two pulses of the same species move toward one another along a depletable nutrient gradient.

Experimentally, external gradients have previously been shown to play an important role in collective behavior of species that move by chemotaxis. For example, it has been shown that a nutrient gradient can give rise to a traveling pulse in a population that moves by chemotaxis [5]. Similar results have been found for temperature and oxygen as well [4,10–12]. An invaluable mathematical tool for studying collective behavior by chemical sensing is the Keller–Segel chemotaxis model. Since its inception, the Keller–Segel model has successfully captured important characteristics of the dynamics of a variety of species, from cellular slime molds such as *Dictyostelium discoideum* to bacteria such as *Escherichia coli*

^{*} Corresponding author.

E-mail address: gsy4@psu.edu (G. Young).

to insects such as the fruit fly *Drosophila melanogaster* [13–17]. Here we use an adaptation of the Keller–Segel model to analyze the transient dynamics of two pulses of bacteria that move toward one another in a one-dimensional nutrient gradient. The pulses are assumed to be maintained by cell–cell interaction via a secreted chemoattractant, while their directional movement follows a nutrient gradient created by the bacteria through consumption. Such a model has been shown in the past to accurately describe the behavior of bacterial pulses in 1-d [4]. Our numerical analysis of this model reveals that at least two outcomes are possible. In the first, the two pulses combine to form a single pulse that moves either to the left or right, depending on initial conditions. In the second, the two pulses initially approach one another but turn around before combining and move in the direction from which they respectively originated.

Pulse-pulse interaction has been studied in a variety of reaction-diffusion systems, including the Gierer-Meinhardt and Gray-Scott models [18-21]. In these works, asymptotic matching is used to derive leading-order ordinary differential equations (ODEs) for the distance between the centers of pulses. The stability of the origin of the resulting ODE determines whether the two pulses are predicted to combine or repel. However, this framework depends heavily on the dynamics of the pulses being slow, and does not allow for analysis of the transient behavior of pulses. Here, we introduce a straightforward heuristic approximation to the spatial profile of each pulse using a Gaussian distribution as a method of moment closure [22]. From this assumption, we are able to derive explicit ODEs describing the dynamics of the centers of mass and the widths of the pulses. In contrast to the Keller-Segel partial differential equation (PDE) model, our ODE model eases linear stability analysis of equilibrium states and numerical simulation and allows phase plane analysis in some situations. In these ways, our approximate model facilitates analysis of the global dynamics of the bacterial system and enables us to efficiently explore qualitative behavior changes across variations of parameters. We show that our approximate model agrees with the Keller-Segel model in predicting that bacterial accumulation is the result of an instability of the uniform state that occurs when the bacterial population size is made sufficiently large. We then define a boundary value problem using our model to analyze parameter conditions that lead to the turnaround of the bacterial populations and conditions that cause them to combine, obtaining mechanistic predictions for future experimental consideration. Finally, we present experimental results that demonstrate that the two behaviors, theoretically predicted by the model, are indeed viable outcomes experimentally as well. The experimental system we use consists of two E. coli populations that are placed on opposite ends of a long channel with a supply of nutrient between them. As a result, bacterial pulses evolve on both ends of the channel and move steadily toward the center of the channel. We track their motion as they travel as pulses toward one another and observe that once the distance between them shrinks sufficiently, they combine and move together in one direction in some cases, or turn around and move back apart in others. These results suggest that the ODE model that we have developed may serve as a useful tool for future studies of bacterial motion.

2. Model derivation and simulation

2.1. Keller-Segel model framework

The Keller–Segel model is a classic partial differential equations model that describes the collective motion of a cellular population that moves by chemotaxis along a chemical gradient created by an attractant produced by the population. In its original and most common form, the model incorporates two modes of motion:

linear diffusion and chemotaxis up the chemical gradient (for a derivation of these dynamics, see, e.g., [13,14]). In its simplest form, the Keller–Segel model is given by

$$\frac{\partial b}{\partial t} = D_b \frac{\partial^2 b}{\partial x^2} - \chi_a \frac{\partial}{\partial x} \left[b \frac{\partial a}{\partial x} \right]
\frac{\partial a}{\partial t} = D_a \frac{\partial^2 a}{\partial x^2} + rb - \delta a,$$
(1)

where b(t, x) represents a bacterial concentration and a(t, x) represents its chemoattractant density at time t and spatial coordinate x [13]. Here we consider an adaptation of the Keller–Segel model to study two interacting pulses of bacteria in a one-dimensional nutrient gradient. We denote the two bacterial concentrations by b(t, x) and $\beta(t, x)$ at time $t \ge 0$ and spatial coordinate $0 \le x \le 0$ L. We assume the bacterial populations diffuse at linear rate D_h . Here we consider the effects of two chemical substances. First, we denote by a(t, x) and $\alpha(t, x)$ the chemoattractant produced by the bacterial populations b(t, x) and $\beta(t, x)$, respectively. The two bacterial populations are assumed to be the same species, and we therefore further assume that both populations are mutually attracted to both chemoattractant concentrations. We assume that the chemoattractant is produced by the bacteria at constant rate r, diffuses at rate D_a , and naturally degrades at rate δ and both bacterial populations are attracted up this chemical gradient at rate χ_a . Second, we include an externally added nutrient, with concentration $\phi(t, x)$, that diffuses at rate D_{ϕ} and the bacteria consume at constant rate κ . Both bacterial populations move up this nutrient gradient at rate χ_{ϕ} . While cellular division has been shown to be a mechanism by which traveling waves can form in Keller-Segeltype models (e.g., [23]), our present focus is on the interaction of bacterial pulses by chemotaxis alone, and we consequently omit bacterial growth from our model [5]. Under these assumptions, the resulting model takes the form

$$\frac{\partial b}{\partial t} = D_b \frac{\partial^2 b}{\partial x^2} - \chi_a \frac{\partial}{\partial x} \left[b \frac{\partial (a + \alpha)}{\partial x} \right] - \chi_\phi \frac{\partial}{\partial x} \left[b \frac{\partial \phi}{\partial x} \right]
\frac{\partial \beta}{\partial t} = D_b \frac{\partial^2 \beta}{\partial x^2} - \chi_a \frac{\partial}{\partial x} \left[\beta \frac{\partial (a + \alpha)}{\partial x} \right] - \chi_\phi \frac{\partial}{\partial x} \left[\beta \frac{\partial \phi}{\partial x} \right]
\frac{\partial a}{\partial t} = D_a \frac{\partial^2 a}{\partial x^2} + rb - \delta a$$

$$\frac{\partial \alpha}{\partial t} = D_a \frac{\partial^2 \alpha}{\partial x^2} + r\beta - \delta \alpha$$

$$\frac{\partial \phi}{\partial t} = D_\phi \frac{\partial^2 \phi}{\partial x^2} - \kappa (b + \beta) \phi$$
(2)

with no-flux boundary conditions

$$\left. \frac{\partial y}{\partial x} \right|_{x=0} = 0 \tag{3}$$

for all $y \in \{b, \beta, a, \alpha, \phi\}$. Parameter descriptions are summarized in Table 1.

We note that if we define $\hat{b} = b + \beta$ and $\hat{a} = a + \alpha$, system (2) can be written as a three-equation system in terms of \hat{b} , \hat{a} , and ϕ . However, we make the distinction between bacterial and chemoattractant concentrations for the sake of distinguishing between populations numerically, and also to simplify the analysis once we introduce an approximation in Section 3.1.

To further ease numerical analysis, we nondimensionalize model (2) as follows:

$$b = N\tilde{b}; \ \beta = N\tilde{\beta}; \ a = K\tilde{a}; \ \alpha = K\tilde{\alpha}; \ \phi = M\tilde{\phi}; \ x = L\tilde{x},$$

where L is the domain length, and N, K, and M are large numbers approximating the maximum size of the bacterial, chemoattractant, and nutrient concentrations, respectively. Here we assume

that $L=20~{\rm cm}, K=M\sim 10^{14}~{\rm cm}^{-1}$ and $N\sim 10^8~{\rm cells~cm}^{-1}$. We provide the details in the supplementary information, and similar nondimensionalization techniques can be found in, e.g., [13]. After nondimensionalization, the parameter values we use are those given in Table 1. The natural dimensions (before nondimensionalization) are included. All nondimensionalized rate parameters have units s^{-1} , and the spatial domain is the unit interval [0, 1]. For simplicity, we immediately replace the nondimensionalized symbols \tilde{b} , $\tilde{\beta}$, \tilde{a} , $\tilde{\alpha}$, $\tilde{\phi}$, and \tilde{x} with b, β , a, α , ϕ , and x, respectively, in the nondimensionalized system. The boundary conditions (3) therefore become

$$\left. \frac{\partial y}{\partial x} \right|_{x=0,1} = 0 \tag{4}$$

for all $y \in \{b, \beta, a, \alpha, \phi\}$.

In the normalized domain, we assume the initial profile of the externally added nutrient is near-uniform in the interior but depleted by the bacteria on the endpoints. In particular, we choose this profile to be given by the reflected sigmoid

$$\phi(0, x) = \begin{cases} F(x - 0.1), & 0 \le x \le 0.5, \\ F(0.9 - x), & 0.5 < x \le 1 \end{cases},$$
 (5)

where $F(x) = \phi_0/(1 + \exp(-100x))$ is a logistic function and ϕ_0 is a parameter. This profile is visualized in Fig S2 in the Supplementary Material.

We choose all model parameters except κ based on those reported in [4] and [5]. The model found in [4] assumes that nutrient consumption is proportional to the bacterial density only, represented by the term $-\kappa b$. Here, we model nutrient consumption with a mass action term proportional to the product of the bacterial density and nutrient, $-\kappa b\phi$ (cf. [2]). This consumption rate can be viewed as an approximation of more detailed consumption terms, such as the common Monod equation, and importantly requires that both bacteria and nutrient be present in order for nutrient to be consumed [24]. The consumption rate parameter used here is therefore much smaller than that found in the literature.

2.2. Numerical results

Here we present simulation results of the two-population Keller–Segel system (2), focusing on two robust behaviors of the system. In each simulation, we initialize the system with the two populations accumulated on opposite ends of the spatial domain. We assume that sufficient time has passed so that the bacteria have consumed the nutrient at the densely populated regions at the ends of the domain so that the nutrient concentration is initially distributed as the symmetric sigmoid function given by Eq. (5). Without the nutrient, the bacterial populations would remain accumulated at their respective ends of the domain, maintaining a concentration of chemoattractant, and would not travel toward each other. Before we present our main numerical results, we briefly review the necessary condition on the Keller–Segel model for pulse-like solutions to form.

To form and maintain a coherent aggregation peak, which call a pulse, the bacterial population size must exceed a critical threshold [4]. If the cell density is too low, the secreted attractant cannot accumulate fast enough to achieve the minimal concentration required for other bacteria to sense it. The Keller–Segel model captures this phenomenon: cellular populations evolving according to this model can only form a nontrivial pulse if the population size is sufficiently large relative to model parameters [6,7,13,14]. Below this critical threshold, the only solution is the uniform solution, $b = b_{tot} = \text{constant}$, $\beta = \beta_{tot} = \text{constant}$, and $a = r(b_{tot} + \beta_{tot})/\delta$. Model (2) in particular predicts that in order to maintain a

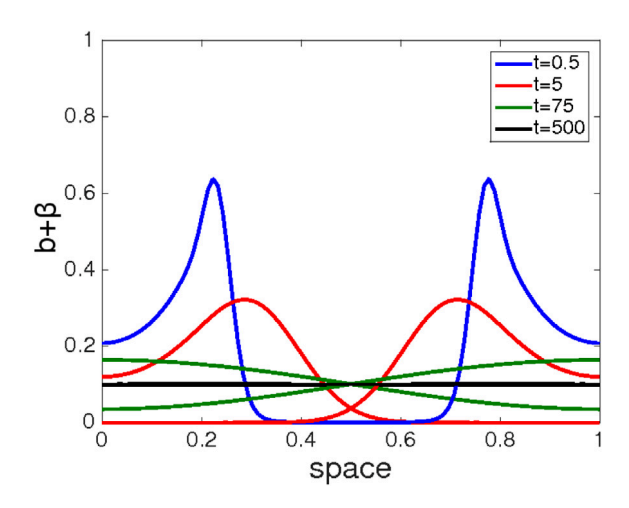


Fig. 1. Bacteria dynamics predicted by the Keller–Segel model with population size below critical threshold (6). The two populations originating at opposite domain boundaries initially move up the nutrient gradient toward each other but cannot maintain pulse-like profiles. Here $b_{tot} + \beta_{tot} = 0.1$, below the critical threshold of $b_{tot}^* + \beta_{tot}^* \approx 0.24$.

nontrivial pulse, the total amount of bacteria must be greater than the critical threshold defined by [6]

$$b_{tot}^* + \beta_{tot}^* = \frac{D_b[\pi^2 D_a + \delta]}{r\chi_a}.$$
 (6)

For the parameters in Table 1, this threshold is $b_{tot}^* + \beta_{tot}^* \approx 0.24$. The nutrient ϕ does not affect the asymptotic stability of the uniform state because it vanishes at steady state. The presence of nutrient can cause transient bacterial pulses to form, but the system will always settle into the uniform state when the total amount of bacteria is below the threshold specified in Eq. (6).

Fig. 1 shows an example of a simulation of model (2) when the combined bacterial population size is less than threshold (6). The two populations initially form pulses and move up the nutrient gradient toward the center, but eventually lose their pulse-like shapes and diffuse out to uniformly fill the spatial domain.

When the total amount of bacteria exceeds threshold (6), the bacterial populations will asymptotically form a pulse along one or both of the boundaries of the spatial domain. We will henceforth only consider bacterial population sizes above this threshold.

We now present our primary numerical result. Figs. 2 and 3 show examples of two striking qualitatively distinct behaviors. Both figures were generated by simulating model (2) with both bacterial and chemoattractant concentrations initially distributed at the one-population, external nutrient-free steady state (with b and a accumulated along the left boundary and β and α along the right). The simulations in the two figures differed only in the initial bacterial population sizes, $b_{tot} = \beta_{tot}$. In Fig. 2, $b_{tot} = \beta_{tot} = 3.2$, and the two bacterial populations move up the nutrient gradient toward one another until they meet and combine into a single pulse. Due to the overall symmetry of the initial conditions, the pulse remains in the center of the domain for roughly ten times longer than it took the pulses to reach the center. The combined pulse eventually propagates to the left end of the domain, due to small asymmetries in the initial conditions or numerical error; noise would also be a factor in corresponding experiments. We note that there is nothing special about the left end of the domain, and that small perturbations to the initial conditions could result in movement to the right end. In Fig. 3, $b_{tot} = \beta_{tot} = 4$, and the two populations again initially move up the nutrient gradient, but eventually change direction and move backwards toward the chemoattractant that is accumulated near the boundaries.

Table 1Parameters used in model (1). The values listed are the nondimensionalized values we use in our simulations, though we list the corresponding pre-nondimensionalization units of each parameter in the "Natural dimensions" column. Before the nondimensionalization procedure described above, all parameters other than κ are based on those measured and fitted in [4] and [5].

	Parameter	Value	Natural dimensions
D_b	Diffusivity of bacteria	0.001	cm ² s ⁻¹
D_a	Diffusivity of attractant	0.03	$\mathrm{cm^2\ s^{-1}}$
D_{ϕ}	Diffusivity of nutrient	0.03	$cm^2 s^{-1}$
Χa	Chemotactic sensitivity to attractant	0.025	$\mathrm{cm^3\ s^{-1}}$
χ_{ϕ}	Chemotactic sensitivity to nutrient	0.015	$\mathrm{cm^3\ s^{-1}}$
r	Production rate of attractant by bacteria	0.05	$cells^{-1} s^{-1}$
δ	Natural decay rate of attractant	0.005	s^{-1}
κ	Consumption rate of nutrient by bacteria	0.001	$(cells/cm)^{-1} s^{-1}$
ϕ_0	Initial nutrient abundance parameter	20	Dimensionless

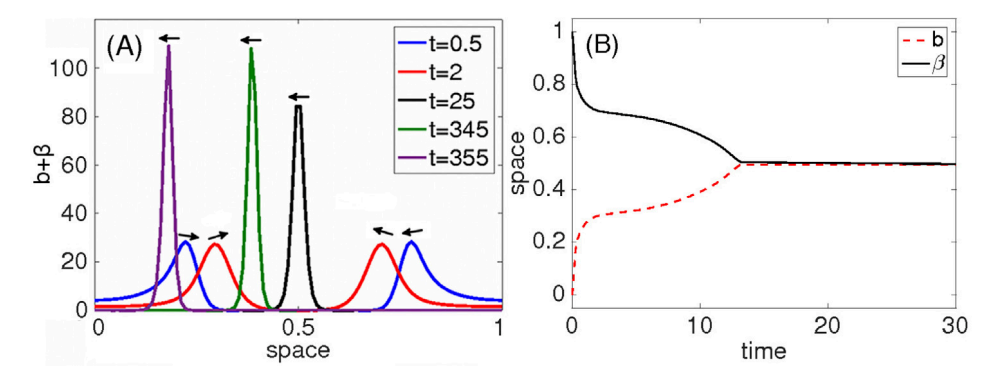


Fig. 2. Bacterial pulses combining under the dynamics of system (2) with boundary conditions (4) and initial bacterial population size $b_{tot} = \beta_{tot} = 3.2$. (A) Snapshots of the bacterial profiles at different times. The arrows indicate direction of motion. By t = 25, the two populations have combined and begun moving toward the left boundary. (B) The positions of the peaks of the bacterial pulses over time. The visualized time period only includes an early window after the pulses combine, excluding the long pause before the two peaks eventually move to the left end of the domain. See Fig S3 in the Supplementary Material for visualization of the chemoattractant and nutrient profiles.

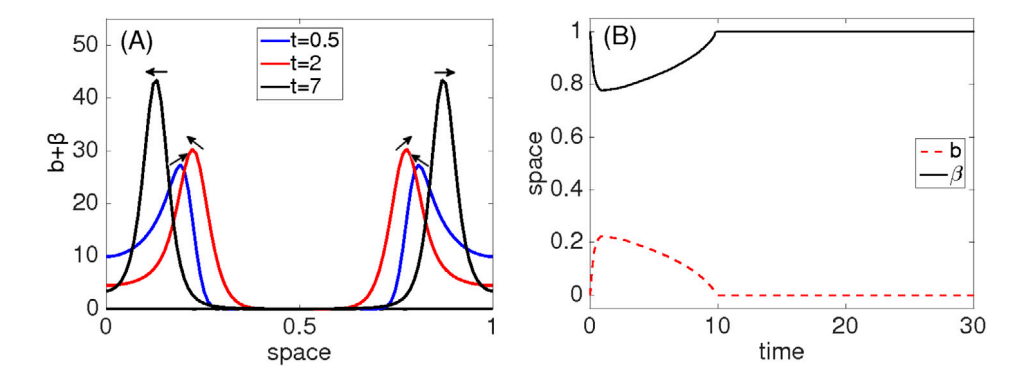


Fig. 3. Bacterial pulses turning around under the dynamics of system (2) with boundary conditions (4) and initial bacterial population size $b_{tot} = \beta_{tot} = 4$. (A) Snapshots of the bacterial profiles at different times. Arrows indicate direction of motion. (B) The positions of the peaks of the bacterial pulses over time. See Fig S4 in the Supplementary Material for visualization of the chemoattractant and nutrient profiles.

Though the distinction between these outcomes results from a change in the bacterial population size, we note that we can produce similar results by changing other model parameters. For example, if we start from conditions that result in the two populations combining, reducing the initial abundance of the nutrient results in both populations turning around (data not shown).

We seek to understand possible mechanisms of these distinct outcomes. We observe that both the combining outcome and the turnaround outcome can be characterized by the relative position of the center of mass of the two bacterial populations: if the centers of mass coalesce, then the two populations have combined; if they change direction and approach the opposite boundaries of the domain, then the two populations have turned around. In the following section, we use a simple approximation to the spatial profile of each population to derive a system of ordinary differential equations (ODEs) describing the dynamics of the size, center

of mass, and variance of the spatial profile of each bacterial pulse. By tracking information about these critical characteristics in an ODE setting, we can much more efficiently explore and generate predictions about parameter-dependence of solution behavior.

3. Moment closure

3.1. Gaussian approximation to the spatial distribution yields an ODE

Here we consider the temporal dynamics of the spatial moments of the bacterial, chemoattractant, and nutrient distributions. Because the pulse–pulse interaction occurs in the interior of the spatial domain, we are concerned with transient behavior of the bacteria away from the spatial boundaries. We therefore remove boundary effects by considering the spatial domain $(-\infty, \infty)$.

Table 2System variables and parameters (dimensionless) used in model (8).

	Variable	Initial condition
b_0, β_0	Total bacteria	3.2 or 4
a_0, α_0	Total chemoattractant	rb_0/δ
ϕ_0	Total nutrient	35
μ_b, μ_β	Center of mass of bacteria	0,1
μ_a, μ_{α}	Center of mass of chemoattractant	0,1
μ_{ϕ}	Center of mass of nutrient	0.5
$\sigma_b^2, \sigma_\beta^2$	Variance of the bacteria profile	0.005
σ_a^2, σ_a^2	Variance of the chemoattractant profile	0.2
$\sigma_b^2, \sigma_\beta^2$ $\sigma_a^2, \sigma_\alpha^2$ σ_ϕ^2	Variance of the nutrient profile	0.1
	Parameter	Value
D_b	Diffusivity of bacteria	10 ⁻⁵
D_a	Diffusivity of attractant	0.0002
D_{ϕ}	Diffusivity of nutrient	0.0002
Χα	Chemotactic sensitivity to attractant	0.00025
χ_{ϕ}	Chemotactic sensitivity to nutrient	0.0002
r	Production rate of attractant by bacteria	0.05
δ	Natural decay rate of attractant	0.005
κ	Consumption rate of nutrient by bacteria	0.001

The *i*th moment of population $s \in \{b, \beta, a, \alpha, \phi\}$ is defined as

$$s_i(t) = \int_{-\infty}^{\infty} x^i s(t, x) dx,$$

for $i=0,1,\ldots$ For each of the five populations s, the quantity s_0 is interpreted as the total amount of s in the system, $\mu_s:=s_1/s_0$ is the location of the center of mass of s, and $\sigma_s^2:=s_2/s_0-(s_1/s_0)^2$ is the variance of the profile of s. Differentiating s_0 , μ_s , and σ_s^2 , for $s\in\{b,\beta,a,\alpha,\phi\}$, with respect to time provides a system of ordinary differential equations describing the temporal dynamics of these variables. For example, the differential equation governing the dynamics of b_0 is

$$\dot{b}_{0} = \int_{-\infty}^{\infty} \frac{\partial}{\partial t} \left[b(t, x) \right] dx$$

$$= \int_{-\infty}^{\infty} \left(D_{b} \frac{\partial^{2} b}{\partial x^{2}} - \chi_{a} \frac{\partial}{\partial x} \left[b \frac{\partial a}{\partial x} \right] - \chi_{\phi} \frac{\partial}{\partial x} \left[b \frac{\partial \phi}{\partial x} \right] \right) dx$$

$$= \left(D_{b} \frac{\partial b}{\partial x} - \chi_{a} b \frac{\partial a}{\partial x} - \chi_{\phi} b \frac{\partial \phi}{\partial x} \right) \Big|_{-\infty}^{\infty}$$

$$= 0$$
(7)

and that of μ_b is

$$\begin{split} \dot{\mu}_{b} &= \frac{d}{dt} \left[b_{1}/b_{0} \right] \\ &= \frac{1}{b_{0}} \int_{-\infty}^{\infty} \frac{\partial}{\partial t} \left[x b(t, x) \right] dx \\ &= \frac{1}{b_{0}} \int_{-\infty}^{\infty} x \left(D_{b} \frac{\partial^{2} b}{\partial x^{2}} - \chi_{a} \frac{\partial}{\partial x} \left[b \frac{\partial a}{\partial x} \right] - \chi_{\phi} \frac{\partial}{\partial x} \left[b \frac{\partial \phi}{\partial x} \right] \right) dx \\ &= \frac{1}{b_{0}} \left[x \left(D_{b} \frac{\partial b}{\partial x} - \chi_{a} b \frac{\partial a}{\partial x} - \chi_{\phi} b \frac{\partial \phi}{\partial x} \right) \Big|_{-\infty}^{\infty} \\ &- \int_{-\infty}^{\infty} (D_{b} \frac{\partial b}{\partial x} - \chi_{a} b \frac{\partial a}{\partial x} - \chi_{\phi} b \frac{\partial \phi}{\partial x}) dx \right] \\ &= \frac{1}{b_{0}} \left[0 - D_{b} b \Big|_{-\infty}^{\infty} + \chi_{a} \langle b a_{x} \rangle + \chi_{\phi} \langle b \phi_{x} \rangle \right] \\ &= \frac{\chi_{a} \langle b a_{x} \rangle + \chi_{\phi} \langle b \phi_{x} \rangle}{b_{0}}, \end{split}$$

where $1/b_0$ factors out because b_0 is a constant by (7), the boundary terms are zero by assumption, and

$$\langle fg \rangle = \int_{-\infty}^{\infty} f(x)g(x)dx.$$

Similarly, differentiating each of the remaining variables produces the following system of fifteen ordinary differential equations:

$$\begin{split} \dot{b}_0 &= 0 \\ \dot{a}_0 &= rb_0 - \delta a_0 \\ \dot{\beta}_0 &= 0 \\ \dot{\alpha}_0 &= r\beta_0 - \delta \alpha_0 \\ \dot{\phi}_0 &= -\kappa \langle b\phi \rangle - \kappa \langle \beta\phi \rangle \\ \dot{\mu}_b &= \frac{\chi_a \langle ba_x \rangle + \chi_a \langle b\alpha_x \rangle + \chi_\phi \langle b\phi_x \rangle}{b_0} \\ \dot{\mu}_a &= \frac{rb_0}{a_0} (\mu_b - \mu_a) \\ \dot{\mu}_\beta &= \frac{\chi_a \langle \beta a_x \rangle + \chi_a \langle \beta \alpha_x \rangle + \chi_\phi \langle \beta \phi_x \rangle}{\beta_0} \\ \dot{\mu}_\alpha &= \frac{r\beta_0}{\alpha_0} (\mu_\beta - \mu_\alpha) \\ \dot{\mu}_\phi &= -\frac{\kappa}{\phi_0} (\langle xb\phi \rangle - \mu_\phi \langle b\phi \rangle) - \frac{\kappa}{\phi_0} (\langle x\beta\phi \rangle - \mu_\phi \langle \beta\phi \rangle) \\ \dot{\sigma}_b^2 &= 2D_b + 2 \\ &\times \frac{\chi_a \langle (x - \mu_b)ba_x \rangle + \chi_a \langle (x - \mu_b)b\alpha_x \rangle + \chi_\phi \langle (x - \mu_b)b\phi_x \rangle}{b_0} \\ \dot{\sigma}_a^2 &= 2D_a + \frac{rb_0}{a_0} \left(\sigma_b^2 - \sigma_a^2 + (\mu_b - \mu_a)^2 \right) \\ \dot{\sigma}_\beta^2 &= 2D_b + 2 \\ &\times \frac{\chi_a \langle (x - \mu_\beta)\beta a_x \rangle + \chi_a \langle (x - \mu_\beta)\beta \alpha_x \rangle + \chi_\phi \langle (x - \mu_\beta)\beta\phi_x \rangle}{\beta_0} \\ \dot{\sigma}_\alpha^2 &= 2D_a + \frac{r\beta_0}{\alpha_0} \left(\sigma_\beta^2 - \sigma_\alpha^2 + (\mu_\beta - \mu_\alpha)^2 \right) \\ \dot{\sigma}_\phi^2 &= 2D_\phi + \frac{\kappa}{\phi_0} \left(\sigma_\phi^2 \langle b\phi \rangle + \sigma_\phi^2 \langle \beta\phi \rangle - \langle (x - \mu_\phi)^2 b\phi \rangle - \langle (x - \mu_\phi)^2 \beta\phi \rangle \right). \end{split}$$

Unless otherwise specified, the parameter values used are those found in Table 2. These values are based on those used in the Keller–Segel model (2), though we must rescale chemotactic sensitivity and diffusivity to maintain similar effects of these parameters on the lengthened spatial scale. The corresponding parameters used in the ODE model (8) are consequently smaller than their counterparts in the PDE model (2).

The nonlinearities within the Keller–Segel model (2) naturally result in mixed moments in system (8). We seek a method of moment closure that does not sacrifice important aspects of the system, namely the pulse-like shape of each population. To this end, we assume that each population maintains a Gaussian profile; that is.

$$s(t,x) = \frac{s_0(t)}{\sigma_s(t)\sqrt{\pi}} \exp\left(\frac{-(x-\mu_s(t))^2}{\sigma_s^2(t)}\right). \tag{9}$$

We note that while we could have chosen as our approximation any function that is pulse-like, such as sech(x), our choice of a Gaussian distribution allows us to explicitly evaluate each integral that appears in system (8).

3.2. Stability of uniform state

We begin our analysis of the approximate model (8) by considering the stability of uniform solutions. A foundational result for the original one-population Keller–Segel model (1) is its ability to explain bacterial pulse formation as a Turing instability of the uniform state. In particular, the size of the bacterial population

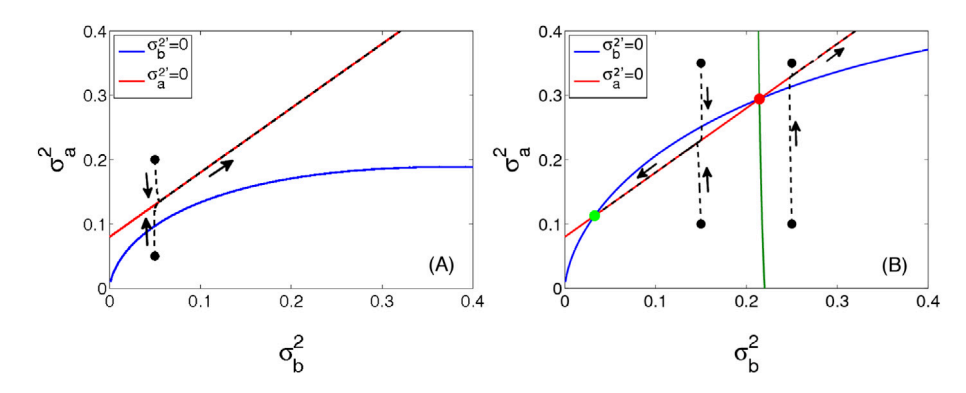


Fig. 4. Phase plane of system (11) describing steady states of the Gaussian approximation model. (A) The bacterial size $b_0=0.008$ is below the critical threshold b_0^* . Trajectories approach the σ_a^2 -nullcline (red) and then both σ_a^2 and σ_b^2 tend to infinity. (B) The bacterial population size $b_0=0.012$ is above the critical threshold b_0^* . The left-most equilibrium point is a stable node (green dot). The right-most equilibrium point is a saddle (red dot), the stable manifold of which is shown as the green curve. To the left of this stable manifold, trajectories tend toward the stable node, and the bacteria consequently form a pulse. To the right of the manifold, trajectories tend to infinity, and the bacteria diffuse out to the uniform solution. Arrows in both panels indicate the direction of flow and the black dots indicate representative initial conditions . (For interpretation of the references to color in this figure legend, the reader is referred to the web version of this article.)

must exceed threshold (6) in order for the bacteria to form and maintain a pulse. To show that system (8) reproduces this result, we consider the *b-a*subsystem of (8), namely

$$\begin{split} \dot{b}_0 &= 0 \\ \dot{a}_0 &= rb_0 - \delta a_0 \\ \dot{\mu}_b &= \frac{\chi_a \langle ba_x \rangle + \chi_a \langle b\alpha_x \rangle + \chi_\phi \langle b\phi_x \rangle}{b_0} \\ \dot{\mu}_a &= \frac{rb_0}{a_0} (\mu_b - \mu_a) \\ \dot{\sigma}_b^2 &= 2D_b \\ &\quad + 2 \frac{\chi_a \langle (x - \mu_b)ba_x \rangle + \chi_a \langle (x - \mu_b)b\alpha_x \rangle + \chi_\phi \langle (x - \mu_b)b\phi_x \rangle}{b_0} \\ \dot{\sigma}_a^2 &= 2D_a + \frac{rb_0}{a_0} \left(\sigma_b^2 - \sigma_a^2 + (\mu_b - \mu_a)^2 \right) \end{split}$$

The differential equation for μ_a indicates that we must have $\mu_b = \mu_a$ at any equilibrium point, but the specific value of these two variables is arbitrary (in other words, the bacterial and chemical pulse must accumulate around the same spatial coordinate, but that coordinate can be anywhere). We therefore introduce the relative coordinate $\mu = \mu_b - \mu_a$. Under this transformation, imposing assumption (9) and evaluating the integrals remaining in the b-a-subsystem in (8) produces

$$\begin{split} \dot{b}_0 &= 0 \\ \dot{a}_0 &= rb_0 - \delta a_0 \\ \dot{\mu} &= \left[\frac{-2\chi_a a_0}{\sqrt{\pi} (\sigma_b^2 + \sigma_a^2)^{3/2}} \exp\left(\frac{-\mu^2}{\sigma_b^2 + \sigma_a^2}\right) - \frac{rb_0}{a_0} \right] \mu \\ \dot{\sigma}_b^2 &= 2D_b - 2\frac{\chi_a a_0 \sigma_b^2}{\sqrt{\pi} (\sigma_b^2 + \sigma_a^2)^{5/2}} \left(\sigma_b^2 + \sigma_a^2 - 2\mu^2\right) \exp\left(\frac{-\mu^2}{\sigma_b^2 + \sigma_a^2}\right) \\ \dot{\sigma}_a^2 &= 2D_a + \frac{rb_0}{a_0} (\sigma_b^2 - \sigma_a^2 + \mu^2). \end{split}$$

From the first two equations, any fixed point of this system must satisfy $a_0^* = rb_0^*/\delta$, where b_0^* is a constant. Since the term inside the brackets in the μ equation is strictly negative, any fixed point must also satisfy $\mu=0$. The remaining two-variable system is

$$\dot{\sigma}_b^2 = 2 \left(D_b - \frac{\chi_a r b_0^* \sigma_b^2}{\sqrt{\pi} \delta (\sigma_b^2 + \sigma_a^2)^{3/2}} \right)$$

$$\dot{\sigma}_a^2 = 2D_a + \delta (\sigma_b^2 - \sigma_a^2).$$
(11)

The generic cases of the nullclines for system (11) are plotted in Fig. 4. In Fig. 4A, the total amount of bacteria is $b_0 = 0.01$ and the system contains no fixed points. The variance of both populations blows up to infinity as time gets large for any initial condition; that is, the bacterial population will always diffuse out into a uniform state if the population size is too low. In Fig. 4B, b_0 is increased to 0.012, and two fixed points exist: a stable node and a saddle point. The stable equilibrium point is analogous to the pulse solution of system (1): the bacterial population and its chemoattractant accumulate around the same center of mass ($\mu = \mu_b - \mu_a = 0$) with a small variance around this point. Starting with a variance in the bacterial population that is too large (that is, to the right of the separatrix of the saddle point), however, results in the variance of both populations increasing without bound. This case is analogous to the system converging to the uniform solution, and so model (10) is generically bistable when b_0 is above a critical threshold.

Fig. 5 shows the saddle-node bifurcation as a function of b_0 , the total amount of bacteria. We can explicitly calculate the critical value of b_0 at which the bifurcation occurs as a function of model parameters. The nullclines of system (11) intersect when

$$D_b - \frac{\chi_a r b_0 \sigma_b^2}{\sqrt{\pi} \delta (2\sigma_b^2 + 2D_a/\delta)^{3/2}} = 0,$$

or equivalently,

$$(\sigma_b^2)^3 + \left(3\frac{D_a}{\delta} - \frac{\chi_a^2 r^2 b_0^2}{8\pi \delta^2 D_b^2}\right) (\sigma_b^2)^2 + \frac{3D_a^2}{\delta^2} \sigma_b^2 + \frac{D_a^3}{\delta^3} = 0.$$
 (12)

When

$$3\frac{D_a}{\delta} - \frac{\chi_a^2 r^2 b_0^2}{8\pi \delta^2 D_b^2} = -\frac{15}{4} \frac{D_a}{\delta},\tag{13}$$

Eq. (12) can be written

$$\left(\sigma_b^2 - 2\frac{D_a}{\delta}\right)^2 \left(\sigma_b^2 + \frac{D_a}{4\delta}\right) = 0,$$

and therefore Eq. (13) is the condition for when the two positive roots of (12) coalesce. This condition gives us the critical bifurcation value for b_0 ,

$$b_0^* = \frac{D_b \sqrt{54\pi D_a \delta}}{r \chi_a}. (14)$$

If $b_0 > b_0^*$, then Eq. (12) has two roots and a stable pulse solution of system (10) exists, and if $b_0 < b_0^*$, then the equation has no roots and the uniform state is the only asymptotic solution of the system.

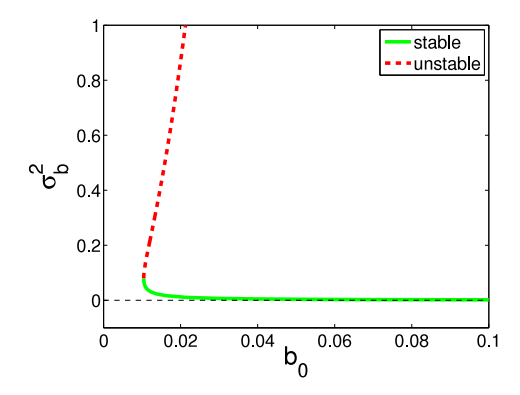


Fig. 5. Bifurcation diagram of system (11). The green curve corresponds to the σ_b^2 coordinate of the stable node, and the red dashed curve corresponds to the σ_b^2 coordinate of the saddle point. The σ_b^2 coordinate of the saddle point increases rapidly with b_0 , and consequently the separatrix in Fig. 4 gets pushed farther to the right, promoting pulse formation . (For interpretation of the references to color in this figure legend, the reader is referred to the web version of this article.)

Comparison to the critical value of b^{tot} in the Keller–Segel system (1),

$$b^{tot} = \frac{D_b(\pi^2 D_a + \delta)}{r \chi_a},$$

shows that a change in any of the model parameters for (10) produces the same qualitative effect on the critical value as in the PDE system (1) (e.g., increasing D_b increases the critical value while increasing r lowers the value), though the critical value scales differently in D_a and δ .

3.3. Numerical simulations of system (8)

As with model (2), we will henceforth only consider regimes under which the bacterial population maintains a size above the critical threshold b_0^* and can therefore sustain a pulse. We further assume symmetric initial conditions, with $b_0(0) = \beta_0(0)$ and $a_0(0) = \alpha_0(0)$, and that $\mu_b(0) = \mu_a(0) = 0$, $\mu_\phi(0) = 0.5$, and $\mu_{\beta}(0) = \mu_{\alpha}(0) = 1$. Two example outcomes of simulations of model (8) demonstrating the observed outcomes from the Keller-Segel model (2) are shown in Figs. 6 and 7. The only difference between the two simulations is bacterial population sizes, $b_0(t) =$ $b_0(0)$ and $\beta_0(t) = \beta_0(0)$, which we assume are much greater than the critical threshold b_0^* in order to guarantee a robust pulse. In Fig. 6, $b_0(0)=\beta_0(0)=3.2$ and the two populations combine and remain stationary after combination. This is in contrast with Fig. 2, in which the combined population moved toward the left end of the domain. System (8) is on the spatial domain $(-\infty, \infty)$, however, such that the combined population does not have a boundary to travel toward and remains stationary once the centers of mass of the two bacterial populations and their respective chemoattractant densities coalesce. In Fig. 7, $b_0(0) = \beta_0(0) = 4$, and the two populations turn around. The parameters chosen in both simulations are those in Table 2. The results shown in Figs. 6 and 7 are consistent with the results from simulations of the Keller-Segel model (2): increasing the initial amount of nutrient causes the bacteria to switch from a regime in which they turn around to one in which they combine (please compare to Figs. 2 and 3). We note that while we have assumed that the two population profiles are initially symmetric in size and width, small asymmetries do not affect the qualitative transient behavior (results not shown).

3.4. Mechanism for turnaround

Our simulations confirm that a change to the population sizes can cause a change in the outcome of the bacterial interaction in our simplified model, just as an analogous change caused varied outcomes in the PDE model. Variations in other parameters and initial conditions, such as the diffusivity of the medium in the channel and the initial abundance of nutrient, can have similar effects on the behavior of the bacterial pulses. In considering whether a bacterial population turns around, we are particularly concerned with the behavior of the center of mass of the population, μ_b . One significant advantage of model (8) over the two-population Keller–Segel model (2) in this regard is that model (8) explicitly includes the time derivative of this center of mass and thus allows us to separately consider the effects that the chemotactic attraction to the chemoattractant and to the nutrient have on its motion.

For example, consider the differential equation for μ_b , which is

$$\dot{\mu}_{b} = \frac{\chi_{a} \langle ba_{x} \rangle + \chi_{a} \langle b\alpha_{x} \rangle + \chi_{\phi} \langle b\phi_{x} \rangle}{b_{0}}
= -\frac{2\chi_{a}a_{0}(\mu_{b} - \mu_{a})}{\sqrt{\pi}(\sigma_{b}^{2} + \sigma_{a}^{2})^{3/2}} \exp\left(\frac{-(\mu_{b} - \mu_{a})^{2}}{\sigma_{b}^{2} + \sigma_{a}^{2}}\right)
- \frac{2\chi_{a}\alpha_{0}(\mu_{b} - \mu_{\alpha})}{\sqrt{\pi}(\sigma_{b}^{2} + \sigma_{\alpha}^{2})^{3/2}} \exp\left(\frac{-(\mu_{b} - \mu_{\alpha})^{2}}{\sigma_{b}^{2} + \sigma_{\alpha}^{2}}\right)
- \frac{2\chi_{\phi}\phi_{0}(\mu_{b} - \mu_{\phi})}{\sqrt{\pi}(\sigma_{b}^{2} + \sigma_{\phi}^{2})^{3/2}} \exp\left(\frac{-(\mu_{b} - \mu_{\phi})^{2}}{\sigma_{b}^{2} + \sigma_{\phi}^{2}}\right),$$
(15)

where each of the three terms in the sum on the right hand side of (15) can be interpreted, in order, as the rate of change in position of the center of mass of b due to its own chemoattractant, due to the other population's chemoattractant, and due to the nutrient. If we denote the distance between the center of mass of the bacterial pulse b and that of any of the attracting substances by x and the sum of the variances of the bacterial population and the same substance by y, then the rate of change of μ_b due to that substance is of the form $(x/y^{3/2}) \exp(-x^2/y)$. Thus, if the centers of mass of the bacterial pulse and an attractant lie at the same position, then the bacterial population experiences no chemotactic pull due to that attractant. If the distance between the pulses is large, the chemotactic pull is exponentially small but nonzero. The chemotactic attraction is maximized with respect to distance x when the two pulses are a small but nonzero distance away from one another. For small variances, the two pulses must be very close in order to provide a large chemotactic attraction. This makes sense, since if both populations are accumulated in very tight pulses, the overlap between the two will be minimal, and consequently the chemical gradient sensed by the bacteria will be small. If the variance of either population is large, however, then even if the distance between the two pulses is large, the pulses can overlap nontrivially, and the bacteria will be attracted up the chemical gradient.

Since we assume that $\mu_b(0)=\mu_a(0)=0$, $\mu_\phi(0)=0.5$, and $\mu_\beta(0)=\mu_\alpha(0)=1$, we have that $\dot\mu_b(0)>0$ and $\dot\mu_a(0)=0$. The center of mass of the bacteria is therefore generically ahead (with respect to the direction of motion) of the center of mass of the chemoattractant for early time. We can now apprehend the mechanism that allows for the bacteria to turn around: the bacteria are attracted inward toward the nutrient and the second population's chemoattractant and outward by their own chemoattractant. If the outward attraction becomes stronger than the inward attraction, then the bacteria will turn around.

Upon inspecting Eq. (15), it is clear that the chemotactic pull toward any given substance is related to the chemotactic sensitivity to the substance (χ_a and χ_ϕ), the distance between the center

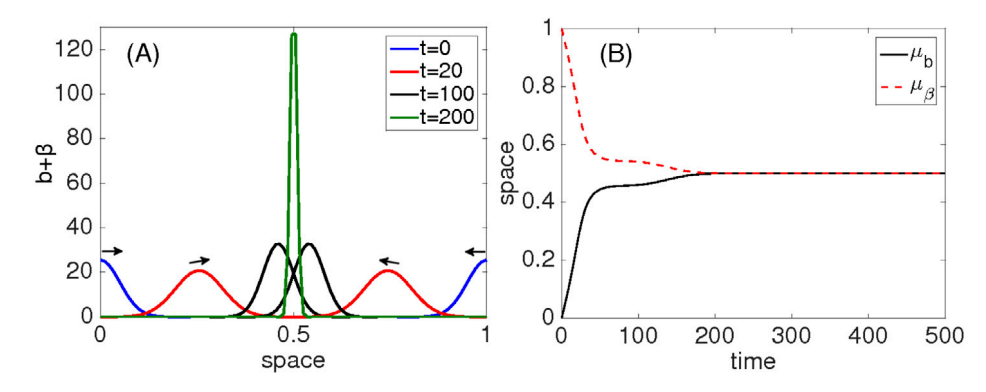


Fig. 6. Bacterial pulses combine under the dynamics of system (8). The two populations move toward one another up the nutrient gradient until they collide and combine to form a single pulse. The bacterial population sizes were $b_0(0) = \beta_0(0) = 3.2$. (A) Snapshots of the bacterial spatial profiles at different times, given by (9). The arrows indicate direction of motion. (B) The positions of the peaks of the bacterial pulses over time. See Fig S5 in the Supplementary Material for visualization of the chemoattractant and nutrient profiles.

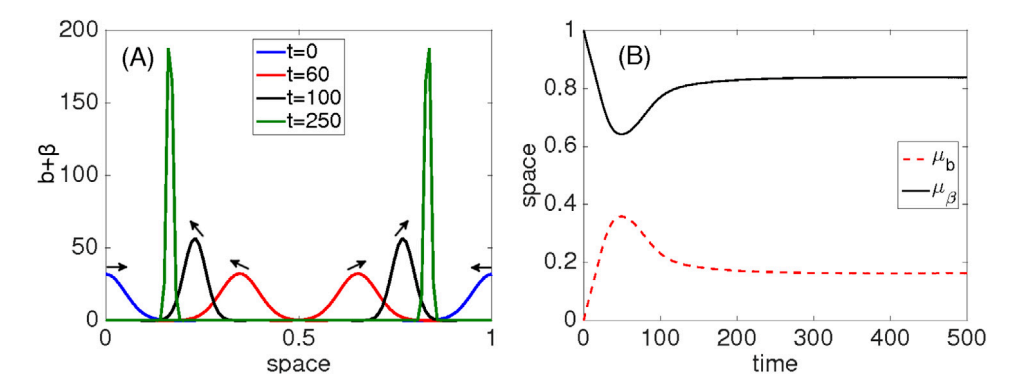


Fig. 7. Bacterial pulses turn around under the dynamics of system (8). The two populations initially move toward one another up the nutrient gradient but later change direction and move back toward their own accumulated chemoattractant. The bacterial population sizes were $b_0(0) = \beta_0(0) = 4$. (A) Snapshots of the bacterial spatial profiles (9) at different times. The arrows indicate direction of motion. (B) The positions of the peaks of the bacterial pulses over time. See Fig S6 in the Supplementary Material for visualization of the chemoattractant and nutrient profiles.

of mass of the bacterial population and that of the substance, the variance of the pulse of the substance, and the total amount of the substance present. Since the latter three quantities are dynamic variables, direct analysis of their effects on the transient behavior of μ_b is not viable. Instead, we consider the effects of parameters related to the dynamics of these variables.

3.5. Capturing turnaround

Our goal in studying system (8) is to determine parameter conditions under which the two populations combine and those under which they turn around. Straightforward analysis of system (8) reveals that, asymptotically, $\mu_b = \mu_\beta$; that is, the two bacterial pulses will always combine in large time, in contrast to solutions of the Keller-Segel model (2). We therefore must take care in deciding what qualifies as a turnaround in model (8). One possible condition is that $\dot{\mu}_b(t_1) = 0$ and $\dot{\mu}_\beta(t_2) = 0$ for some times t_1 and t_2 (indicating that the centers of mass of both populations have changed direction). However, this condition is not sufficient to determine when the populations turn around and move away from one another. Fig. 8 shows an example where both populations quickly turn around but shortly thereafter turn back around and combine. Though the center of mass of each population does change direction in this example, the overall outcome is not compatible with turnaround observed in simulations of the Keller-Segel model, in which the two populations accumulate along

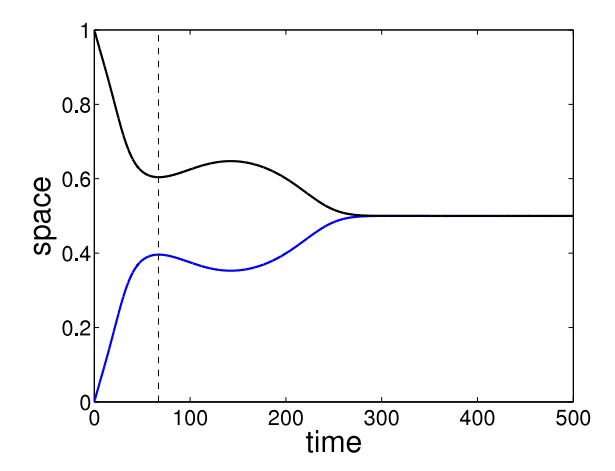


Fig. 8. False turnaround. The vertical dashed line marks a turnaround in the center of mass of both populations, but the populations combine together a short time

opposite ends of the domain. We therefore adopt a more robust but subjective criterion for turnaround.

To arrive at this criterion, we first consider the equation defining the dynamics between the two bacterial pulses in system (8), say $\mu_{b\beta}=\mu_b-\mu_\beta$ with the additional assumption that $\mu_b=\mu_a$ and $\mu_\beta=\mu_\alpha$. The latter assumption allows us to study the pulsepulse interaction without the influence of transient behavior. The

differential equation governing the dynamics of $\mu_{b\beta}$ is then

$$\begin{split} \dot{\mu}_{b\beta} &= \left(-\frac{2\chi_a r \beta_0}{\delta\sqrt{\pi}(\sigma_b^2 + \sigma_\alpha^2)^{3/2}} \exp\left(\frac{-\mu_{b\beta}^2}{\sigma_b^2 + \sigma_\alpha^2}\right) \right. \\ &\left. -\frac{2\chi_a r b_0}{\delta\sqrt{\pi}(\sigma_\beta^2 + \sigma_a^2)^{3/2}} \exp\left(\frac{-\mu_{b\beta}^2}{\sigma_\beta^2 + \sigma_a^2}\right) \right) \mu_{b\beta}. \end{split}$$

Note that the chemotactic attraction of a bacterial population decays exponentially with the distance between the center of mass of the bacteria and that of the chemoattractant. Thus, if the two bacterial populations are sufficiently far apart, then the chemotactic pull from each pulse of chemoattractant to the more distant bacterial population is negligible, and the populations can separately approach a meta-stable state: each population develops into its own pulse-like structure, subject to only an exponentially small effect from the other population's chemoattractant. This state is intuitively consistent with the outcome of the Keller-Segel model in which the two bacterial populations accumulate along the boundaries of the domain. In asymptotic time, the two populations will combine, but the farther apart the two populations are, the longer it will take for the combination to occur. Once the populations do become sufficiently close, however, the relative effect that each population experiences from the other population's chemoattractant becomes nontrivial, and they combine together relatively quickly. We hence reason that if the two populations have not combined after a large but finite amount of time, they must be in a meta-stable non-combined state. We therefore take as our condition for turnaround that the centers of mass of the two populations are distinct after a large amount of time; that is, that $|\mu_b(t_c) - \mu_\beta(t_c)| > \epsilon$ for some small, fixed distance ϵ at some large time $t = t_c$.

We must take care in choosing values for ϵ and t_c . For instance, to establish a boundary between the turnaround outcome and the combination outcome, we must choose ϵ small enough so that the two populations will quickly combine if their center of masses are ϵ apart. We determine through numerical simulation that when the distance between the center of masses reaches $\epsilon=0.1$, that distance decreases monotonically and quickly. Similarly, we must choose t_c large enough to guarantee that the system has in fact reached a meta-stable state and to avoid a false turnaround, as illustrated in Fig. 8. Fig. 9 shows the time $t = t_c$ at which the two populations will be $\epsilon = 0.1$ apart over varied parameter values based on direct simulations. In each panel, the curve defines a boundary. For example, if $\phi_0(0)$ is to the right of the curve in the first panel, then the two populations will be ϵ apart sooner than t_c . In each case, the curve becomes very steep near a critical parameter value. Consequently, as long we choose t_c sufficiently large that the boundary curve is approximately vertical at $t = t_c$, our choice will not have much impact on the parameter value that defines our boundary. Guided by this reasoning, we choose to take as our condition for turnaround that the centers of the two populations are $\epsilon = 0.1$ units away from one another at time $t_c = 500$.

To apply this condition, we solve a modification of system (8) as a boundary value problem (BVP) with boundary condition $|\mu_b - \mu_\beta| = \epsilon = 0.1$ at time $t = t_c = 500$. To satisfy all boundary conditions, we must consider one of the pertinent parameters as a stationary variable, as in [25]. For example, to determine the effect of χ_a on the transient behavior, we include the differential equation $\dot{\chi}_a = 0$ in the BVP system. We then use the continuation software AUTO to solve this BVP across values of the selected parameter [26]. The solution curve in parameter space defines a boundary between regions in which our model predicts that the bacteria turn around and in which it predicts that they combine.

Fig. 10 shows the results of solving this boundary value problem. In this figure, we denote the equal size of the two bacterial populations by $N_0 := b_0 = \beta_0$, the diffusivity of the bacteria by $D = D_b$, and we assume that $D_a = D_\phi = 20 \times D$. Each panel shows a given parameter space divided into two regions. Parameter pairs chosen from the gray region in each panel represent a regime in which the two bacterial populations turn around; parameters chosen from the white region correspond to a regime in which they combine. These figures provide a picture of the relative contributions of the parameters considered. For example, Fig. 10A shows that if the bacterial population size is increased, then more nutrient is needed to induce the bacterial populations to combine. This is easy to understand: if the bacterial populations are larger, then they produce more chemoattractant, and the outward attraction toward the bacteria's own chemoattractant will be stronger, such that combination requires a stronger inward attraction toward the nutrient.

Fig. 10B and C are more subtle. Increasing D can be interpreted as, for example, decreasing the viscosity of the medium in which the bacteria are suspended, thereby increasing the diffusivity of the bacterial and chemical populations. Fig. 10B shows that the higher the diffusion rate, the less initial nutrient is necessary to cause the bacterial population to combine. For too fluid of a medium, the chemoattractant of both populations spreads quickly across the spatial domain to reach the other population. This results in a mutual attraction of both populations toward one another, and the nutrient is no longer needed to pull both populations inward. Fig. 10C similarly shows that in order for the two populations to turn around when diffusivity is high, they need a large initial population size, which provides a large initial supply of chemoattractant. We note that this result only holds for small diffusivity. For diffusivity sufficiently large, both bacterial populations will not be able to maintain a pulse-like shape and will simply diffuse out.

Fig. 10D shows the chemotactic sensitivity of the bacteria toward the chemoattractant, χ_a , versus the sensitivity toward the nutrient, χ_ϕ . While these parameters are unlikely to change naturally, this figure is easily interpreted and agrees with intuition: a strong attraction toward the nutrient will always result in the bacterial populations being pulled quickly inward and combining. If the attraction toward the chemoattractant is sufficiently high relative to the attraction toward the nutrient, then the bacteria will be pulled strongly outward toward the previously accumulated chemoattractant located closer to its initial position and hence the pulses will turn around.

Fig. 10A and D agree with the results of the PDE model (2), visualized in Figs. 2 and 3: increased population size increases the likelihood of the two populations turning around. While we do not visualize the results of the PDE model for any other parameter, we confirmed by direct simulation that for the PDE model, the transitions in dynamics observed by analogous parameter changes (increases or decreases) agree with those shown in Fig. 10.

4. E. coli dynamics in vitro

Now that we have shown that our mathematical model predicts several distinct spatiotemporal behaviors, we consider the types of bacterial motion seen in a corresponding experimental setting.

4.1. Experimental methods

Wild type *Escherichia coli* (*E. coli*) RP437, expressing either yellow fluorescent protein (YFP) or red fluorescent protein (td-Tomato) from a medium copy number plasmid (pZA) under the control of the constitutive λ -Pr promoter, were grown in M9 minimal medium supplemented with 1 g/l casamino acids, and 4 g/l glucose (M9CG) at 30 °C until early exponential growth phase (Optical Density at 600 nm (OD $_{600 \text{ nm}}$) = 0.1) [27]. The cultures were then centrifuged for 5 min at 10,000 rpm, and

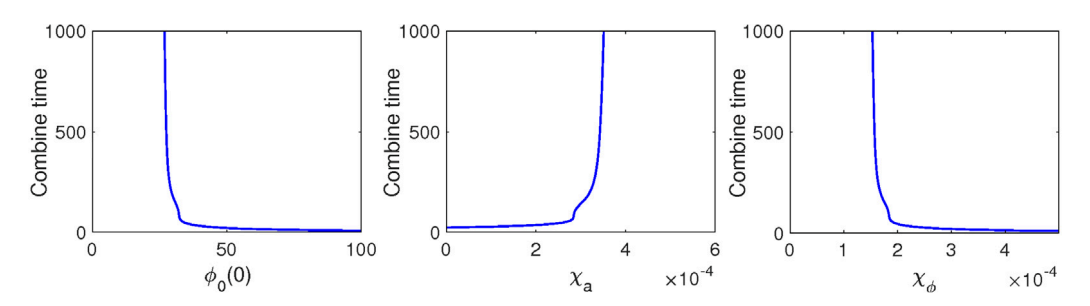


Fig. 9. Dependence of time to combine on model parameters. For the centers of mass of the two bacterial populations to be $\epsilon = 0.1$ space units apart at time t, the parameter on the horizontal axis must take the value specified by the curve. Sensitivity of the time to combine, t_c , on each parameter considered decreases once t_c exceeds some quantitative threshold. Similar figures for parameters N_0 and D not shown.

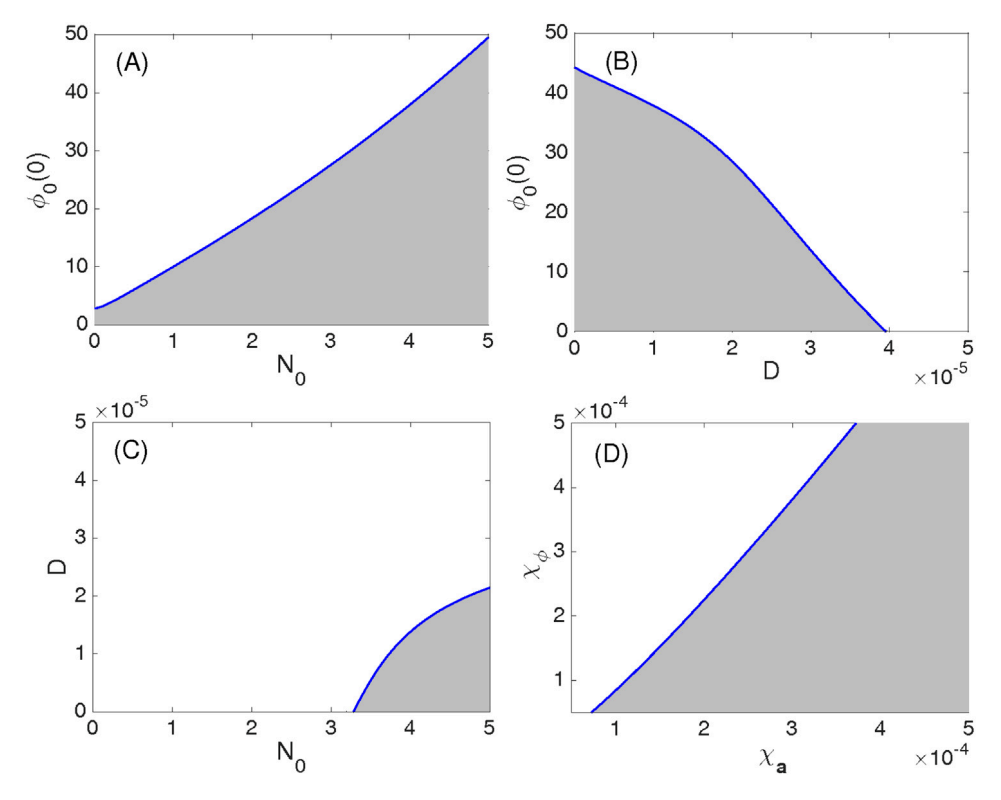


Fig. 10. Boundaries in parameter space between combination (white) and turnaround (gray). The criterion for combination is $\mu_b - \mu_\beta = 0$ before t = 500. Whenever a parameter is not varied, the common bacterial population size $N_0 = 3$, while $D = 10^{-5}$, $\chi_a = 0.00025$, $\chi_\phi = 0.0002$, and $\phi_0(0) = 35$.

resuspended in fresh M9CG medium at an $OD_{600 \text{ nm}} = 0.3$. Each of the bacterial cultures was loaded onto one end of a set of \sim 2 cm long, thin channels (800 μm wide, 20-25 μm deep) fabricated in polydimethylsiloxane (PDMS) and adhered to a microscope glass slide (Fig. 11). The channels were pre-filled with fresh M9CG medium. The bacteria on both ends of the channel were allowed to migrate into the channel. The channel was then sealed on both ends with an epoxy glue to prevent any flow through the channel during observations. This method was successfully used in a previous study [4], and the absence of a flow was confirmed by adding latex beads to the medium and observing their motion to verify that it is diffusive. The sample was then mounted onto an inverted microscope (Zeiss Axiovert 40 CFL), and the bacteria were observed at room temperature (~ 22 °C) in fluorescence mode using a 2.5× objective. Shortly after sealing the channel ends (\sim 10 - 20 min), a sharp accumulation peak appeared at each end of the channel. The peaks are due to cell-cell signaling, likely via the secretion of and attraction to glycine (see Fig S1 in the Supplementary Material). These peaks then proceeded to advance as a pulse toward the center of the channel following a nutrient

gradient created by the bacterial nutrient consumption at the densely populated ends (for more details about this phenomenon see for example [3–5]). When the two pulses were \sim 4 mm away from each other, their dynamics were recorded, each population in its corresponding fluorescence colors, at a rate of 1 image/9 s using a charge-coupled device (CCD) camera (Progress MF, Jenoptik). The fluorescence profile reflecting the bacterial concentration along the channel was measured using ImageJ (NIH). For each of the examples presented in Video Sets 1-4, the fluorescence intensity is depicted in units of the maximal measured fluorescence at the peak of the concentration and the background was subtracted for better comparison. Note that due to technical limitations of imaging that prevent us from acquiring larger images, Movie Sets 1-4 display only a \sim 3.5 mm long section of the channel where the two populations meet. The integral of the fluorescence intensity profile over the whole range is therefore changing primarily due to new bacteria entering the frame, less so due to bacterial reproduction. Under the experimental conditions used here (culture medium being M9CG and incubation temperature being ~ 22 °C) the reproduction rate of the bacteria is about once every 2 h, whereas

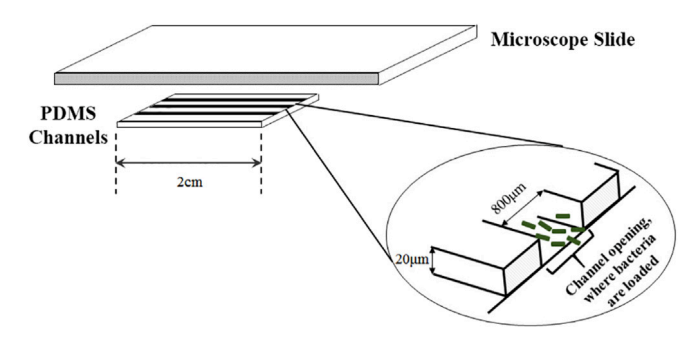


Fig. 11. The experimental setup: a set of narrow channels ($800~\mu m \times 20~\mu m$), 2 cm long, microfabricated with polydimethyl-siloxane (PDMS) using the common techniques [3] and adhered to a microscope slide by plasma cleaning, while leaving both ends open for loading the bacteria. After the bacteria are loaded on both ends, the ends of the channels are sealed via epoxy glue.

the tracking of bacterial positions occurred over periods of less than one hour (e.g., Fig. 12).

4.2. Experimental results

Two bacterial cultures, each expressing a different color fluorescent protein (red or yellow), were loaded onto opposite ends of a long narrow channel filled with M9CG medium (Fig. 11). The bacteria were then observed via fluorescence microscopy at low magnification $(2.5 \times)$ to allow visualization of collective behavior. Our observations reveal that each bacterial population initially accumulates near the end of the channel forming a sharp concentration peak. Each concentration peak then proceeds to propagate as a pulse toward the center of the channel. Subsequently, as predicted by the model, two possible outcomes were observed (Fig. 12A-B). In the first, the two populations combine and either move together toward one end of the channel (Fig. 12A, observed in three out of seventeen experiments) or stay at the collision location, while their accumulation peak reduces in amplitude and widens gradually by diffusion (data not shown, observed in seven out of seventeen experiments). In the second case (Fig. 12B), the two populations' peaks never meet; rather, they approach each other initially and then turn around, with each moving toward the end of the channel where it originated (observed in seven out of seventeen experiments). Additional visualization of these behaviors is provided in the Video Sets 1-4.

While it appears that the initial position of the centers of mass of the bacterial populations differs between Fig. 12A and B, this is not the case and is due to recording limitations. In each experiment, the bacterial populations travel a similar distance before they enter the 3.5 mm section of the channel being recorded, and the asymmetry between initial position in this frame is only due to small differences in arrival time.

5. Discussion

In this paper, we studied the interaction of bacterial pulses in a one-dimensional nutrient gradient. We presented numerical results showing that the classic Keller–Segel model for bacterial chemotaxis predicts that two bacterial populations moving toward one another in a nutrient gradient can change direction and move back in the directions from which they came, rather than continuing toward each other to combine into one unified population. To facilitate analysis of the transient and global dynamics of the system, we developed a system of ordinary differential equations approximating the spatiotemporal dynamics of the spatial moments of each bacterial population and associated attractants represented

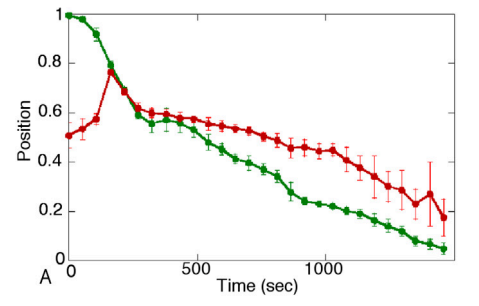
in the Keller–Segel model. Our approximation eases the exploration of effects of parameter variation on population dynamics. After verifying that the approximate model agrees qualitatively with the Keller–Segel model, we defined a condition on model parameters that determines whether the bacterial populations will combine or turn around, then develop and numerically solve a boundary value problem to find the boundary between these two outcomes in various parameter spaces. We end by presenting experimental results that show that two populations of *E. coli* behave according to the predictions of our model when moving toward one another in a long channel.

Our results leave us with predictions about the mechanisms by which the E. coli populations manage to turn around and move away from each other and the nutrient gradient. Model (8) shows that the center of mass of a bacterial population is generically between the center of mass of its chemoattractant and that of the nutrient early in the experiment. This relationship allows the bacteria to turn around if the outward attraction toward the chemoattractant becomes stronger than the inward attraction toward the nutrient. Outward attraction can overcome inward attraction in a number of ways. For example, if the amount of nutrient between the bacterial populations is small, it is likely to yield a small attractive gradient and hence the bacteria will turn back toward the chemoattractant. Our model predicts that if the medium in which the bacteria are suspended is too fluid, then the two bacterial populations will likely combine, because the chemoattractant will spread across the spatial domain, removing the driver of the direction reversal. Variations in the total amount of available nutrient or fluidity of the medium can therefore lead to qualitative changes in the behavior of the bacteria.

We note here that both the PDE and ODE models can produce the turnaround behavior with only a single population. The turnaround behavior occurs when the outward attraction of the chemoattractant gradient overcomes the inward attraction of the nutrient gradient, and a second population is not necessary to achieve this outcome. However, the two-population scenario elucidates that turnaround can still happen despite the additional inward pull of the second population's chemoattractant and alteration of the nutrient gradient, and also captures the combination outcome.

The systematic predictions made by our approximate system agree qualitatively with specific simulations of the Keller–Segel model. Figs. 2 and 3 provide particular examples in which increasing the bacterial population sizes causes the bacterial pulses to switch from a combination outcome to a turnaround outcome. Similarly, increasing the diffusivity of all three populations results in the bacterial populations combining (results not shown). Moreover, we compare the nutrient and chemoattractant profiles from the Keller–Segel model and our approximate system in Figs S3–S6 in the Supplementary Material S1_Text. The figures show that our approximate system preserves key symmetries observed in simulations of the Keller–Segel model and qualitatively match the profiles from the full PDE model. This agreement suggests that our Gaussian approximation system represents a reasonable source of predictions to be tested experimentally.

Seven out of the seventeen experimental trials resulted in the two populations combining then gradually diffusing out. In contrast, pulses formed in both the Keller–Segel model (2) and our approximated model (8) remain formed for all time. This discrepancy is a result of simplifying assumptions in model (2). To produce chemoattractant, *E. coli* require a source of nutrition: in the absence of a nutrient, the bacteria will stop producing chemoattractant, and consequently any pulse formed will simply diffuse out [28]. Model (2), and consequently the approximated model (8), assumes that chemoattractant production is proportional to only the bacteria, not to the nutrient concentration. This is a common assumption



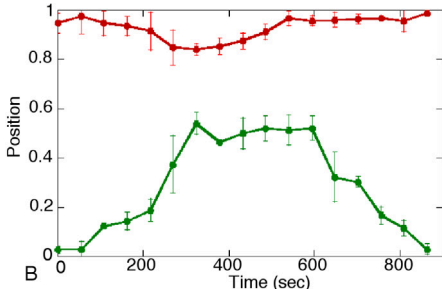


Fig. 12. Experimental results. Example curves showing the position of the centers of mass of the two bacterial pulses throughout their interaction in two cases: combining and moving together to the left (A), and turning around and each moving back toward its original end of the channel (B); note that the left end is at x = 0 and right is at x = 1. The position of each pulse's center of mass was calculated using the 10% densest (highest fluorescence intensity) region for each color bacterium. The error bars represent the standard deviation of the center of mass. The horizontal axis depicts the position scaled between 0 and 1, where 0 is the left end of the channel and 1 is the right end, separated by 3.5 mm from each other. Movies of the experiments and the fluorescence intensity profiles are provided in Video Sets 1-4. (For interpretation of the references to color in this figure legend, the reader is referred to the web version of this article.)

that greatly simplifies the analysis of pulse formation [5,6,13]. On the other hand, including nutrient-dependent chemoattractant production, as in the chemotaxis models found in [7,29], reproduces the experimentally observed outcome in which the bacterial pulse eventually diffuses out, after consuming the nutrient past a critical threshold. Because the time necessary for the bacteria to consume the nutrient past this threshold is longer than the time necessary for the two pulses to either combine or turn around, our analytical results describe the transient behavior of the biological system while nutrient is abundant, and the omission of nutrient-dependent chemoattractant production in the model is reasonable.

Our analysis of the two-population system assumes that both bacterial populations are of equal size. This assumption reduces the number of free parameters but might be unrealistic, as population size could vary between the two populations during an experiment. Simulations of system (8) with unequal but similar population sizes agree qualitatively with those presented in this paper, and the various forms of dynamics we observed therefore do not result from a perfect symmetry in the populations. We also omitted stochastic effects that would be present experimentally. We speculate that such stochasticity would greatly reduce the delay between the combining of pulses and the onset of the drift of the combined pulse arising in our simulations (Fig. 2), presumably representing a manifestation of metastability, but not in experiments (Fig. 12). Moreover, we note that despite the delay between combination and drift of the pulses in our simulations, the combined pulse moves as fast as the single pulses once it begins moving away from the center, in agreement with the experiments.

Our approximate ODE system and the method used to derive it provide an efficient and tractable framework for analyzing the transient dynamics of complex systems. A similar analysis was conducted in [30], in which the authors used singular perturbation techniques to derive a Lotka–Volterra-like ODE competition model between invasive bacteria and host leukocytes from a Keller–Segel system adapted to model the inflammatory response due to bacterial infection. The resulting system allowed the authors to conduct an analysis of global behavior as a function of model parameters but removed all spatial aspects of the system. Our approximation preserves the spatial dimension by considering the temporal dynamics of the key quantities that characterize spatial features of our model populations.

There are several open directions related to this study. On the experimental side, our model yields several predictions about how the outcome of the pulse interaction experiments is expected to depend on aspects of the experimental set-up, such as nutrient concentration and medium viscosity. Future experiments can be used to test these predictions and to guide a more accurate quantitative tuning of our model, which would in turn lead to more precise predictions. On the theoretical side, a natural extension would

be to explore other, more quantitatively accurate approximations to the population distributions. While the bacteria maintains a Gaussian pulse-like distribution in the Keller-Segel model, the chemoattractant and nutrient populations do not necessarily do the same, especially as the two populations interact. One could impose a different assumption on the distributions of the chemical concentrations, the results of which could be important in understanding details of transient behaviors. Similarly, the experimental set-up discussed in this paper did not allow for measurement of nutrient profiles, and it would also be of interest to explore the effects of different initial nutrient distributions on the bacterial dynamics that emerge. Our heuristic approximation could also easily be applied as a method of moment closure for other spatiotemporal models whose nonlinearities make parameter exploration and transient analysis tedious or impossible. Care must be taken when approximating a pulse by a Gaussian distribution, however. In [4] and [5], the bacterial pulses observed were asymmetrical, making a Gaussian a bad fit. In such cases, the spatial profiles can be approximated using parameterized non-Gaussian functions allowing one to derive ODE systems for profile parameters, but the added asymmetry would likely forfeit the analytical advantage of being able to compute the integrals in system (8). Finally, it would be interesting to apply our Gaussian approximation method to a twodimensional Keller-Segel model and explore transient dynamics, asymptotic states, and pattern formation. Our methods could also be used or extended for the study of bacterial interactions in other spatial domains or scenarios, perhaps taking into account changing environmental conditions.

Acknowledgments

The authors acknowledge the support of the National Science Foundation grant awards PHY1401576 (HS), DMS1219753 (GBE), DMS1712922 (GBE), DMS1312508 (JER), and DMS1612913 (JER).

Appendix A. Supplementary data

Supplementary material related to this article can be found online at https://doi.org/10.1016/j.physd.2019.02.007.

References

- [1] Eshel Ben-Jacob, Inon Cohen, András Czirók, Tamás Vicsek, David L Gutnick, Chemomodulation of cellular movement, collective formation of vortices by swarming bacteria, and colonial development, Physica A 238 (1–4) (1997) 121, 107
- [2] Casimir Emako, Charlène Gayrard, Axel Buguin, Luís Neves de Almeida, Nicolas Vauchelet, Traveling pulses for a two-species chemotaxis model, PLoS Comput. Biol. 12 (4) (2016) e1004843.

- [3] Sungsu Park, Peter M Wolanin, Emil A Yuzbashyan, Hai Lin, Nicholas C Darnton, Jeffry B Stock, Pascal Silberzan, Robert Austin, Influence of topology on bacterial social interaction, Proc. Natl. Acad. Sci. 100 (24) (2003) 13910–13915.
- [4] Hanna Salman, Anton Zilman, Claude Loverdo, Marie Jeffroy, Albert Libchaber, Solitary modes of bacterial culture in a temperature gradient, Phys. Rev. Lett. 97 (11) (2006) 118101.
- [5] Jonathan Saragosti, Vincent Calvez, Nikolaos Bournaveas, Axel Buguin, Pascal Silberzan, Benoît Perthame, Mathematical description of bacterial traveling pulses, PLoS Comput. Biol. 6 (8) (2010) e1000890.
- [6] Leah Edelstein-Keshet, Mathematical Models in Biology, Vol. 46, Siam, 1988.
- [7] James D. Murray, Mathematical Biology I. An Introduction, third ed., in: Interdisciplinary Applied Mathematics, vol. 17, Springer, 2002.
- [8] David G Davies, Matthew R Parsek, James P Pearson, Barbara H Iglewski, J William Costerton, E Peter Greenberg, The involvement of cell-to-cell signals in the development of a bacterial biofilm, Science 280 (5361) (1998) 295–298.
- [9] Leslie A Pratt, Roberto Kolter, Genetic analysis of escherichia coli biofilm formation: roles of flagella, motility, chemotaxis and type i pili, Mol. Microbiol. 30 (2) (1998) 285–293.
- [10] Mahmut Demir, Carine Douarche, Anna Yoney, Albert Libchaber, Hanna Salman, Effects of population density and chemical environment on the behavior of escherichia coli in shallow temperature gradients, Phys. Biol. 8 (6) (2011) 063001.
- [11] Carine Douarche, Axel Buguin, Hanna Salman, Albert Libchaber, E. coli and oxygen: a motility transition, Phys. Rev. Lett. 102 (19) (2009) 198101.
- [12] Hanna Salman, Albert Libchaber, A concentration-dependent switch in the bacterial response to temperature, Nat. Cell Biol. 9 (9) (2007) 1098.
- [13] Thomas Hillen, Kevin J Painter, A user's guide to pde models for chemotaxis, J. Math. Biol. 58 (1–2) (2009) 183.
- [14] Dirk Horstmann, From 1970 until present: the keller-segel model in chemotaxis and its consequences. ii, jahresber, Deutsch. Math.-Verein. 106 (2004) 51–69.
- [15] Evelyn F Keller, Lee A Segel, Initiation of slime mold aggregation viewed as an instability, J. Theoret. Biol. 26 (3) (1970) 399–415.
- [16] Evelyn F Keller, Lee A Segel, Model for chemotaxis, J. Theoret. Biol. 30 (2) (1971) 225–234.

- [17] Marjolein E Lof, Maarten De Gee, Lia Hemerik, Odor-mediated aggregation enhances the colonization ability of drosophila melanogaster, J. Theoret. Biol. 258 (3) (2009) 363–370.
- [18] Arjen Doelman, Tasso J Kaper, Semistrong pulse interactions in a class of coupled reaction-diffusion equations, SIAM J. Appl. Dyn. Syst. 2 (1) (2003) 53– 96.
- [19] S-I Ei, Masayasu Mimura, Masaharu Nagayama, Pulse–pulse interaction in reaction–diffusion systems, Physica D 165 (3–4) (2002) 176–198.
- [20] K Kang, T Kolokolnikov, MJ Ward, The stability and dynamics of a spike in the 1d keller–segel model, IMA J. Appl. Math. 72 (2) (2007) 140–162.
- [21] Wentao Sun, Michael J Ward, Robert Russell, The slow dynamics of two-spike solutions for the gray–scott and gierer–meinhardt systems: Competition and oscillatory instabilities, SIAM J. Appl. Dyn. Syst. 4 (4) (2005) 904–953.
- [22] Christian Kuehn, Moment closurea brief review, in: Control of Self-Organizing Nonlinear Systems, Springer, 2016, pp. 253–271.
- [23] Gregoire Nadin, Benoît Perthame, Lenya Ryzhik, Traveling waves for the keller-segel system with fisher birth terms, Interfaces Free Bound. 10 (4) (2008) 517-538.
- [24] Hal L Smith, Paul Waltman, The Theory of the Chemostat: Dynamics of Microbial Competition, Vol. 13, Cambridge university press, 1995.
- [25] Glenn Young, Bard Ermentrout, Jonathan E Rubin, A boundary value approach to optimization with an application to salmonella competition, Bull. Math. Biol. 77 (7) (2015) 1327–1348.
- [26] Bard Ermentrout, Simulating, Analyzing, and Animating Dynamical Systems: A Guide to XPPAUT for Researchers and Students, Vol. 14, Siam, 2002.
- [27] Rolf Lutz, Hermann Bujard, Independent and tight regulation of transcriptional units in escherichia coli via the lacr/o, the tetr/o and arac/i1-i2 regulatory elements, Nucl. Acids Res. 25 (6) (1997) 1203–1210.
- [28] Elena O Budrene, Howard C Berg, Dynamics of formation of symmetrical patterns by chemotactic bacteria, Nature 376 (6535) (1995) 49.
- [29] R Tyson, SR Lubkin, James D Murray, A minimal mechanism for bacterial pattern formation, Proc. Roy. Soc. Lond. B 266 (1416) (1999) 299–304.
- [30] Wolfgang Alt, Douglas A Lauffenburger, Transient behavior of a chemotaxis system modelling certain types of tissue inflammation, J. Math. Biol. 24 (6) (1987) 691–722.